The Journal of Neuroscience, February 1, 2002, 22(3):1081–1097

Simulations of the Role of the Muscarinic-Activated Calcium-Sensitive Nonspecific Cation Current I_{NCM} in Entorhinal Neuronal Activity during Delayed Matching Tasks

Erik Fransén,[1] **Angel A. Alonso,**[2] **and Michael E. Hasselmo**[3]

[1]*Department of Numerical Analysis and Computer Science, Royal Institute of Technology, S-100 44 Stockholm, Sweden,* [2]*Department of Neurology and Neurosurgery, Montreal Neurological Institute and McGill University, Montreal, QC H3A Canada, and* [3]*Department of Psychology, Program in Neuroscience, and Center for Biodynamics, Boston University, Boston, Massachusetts 02215*

Entorhinal lesions impair performance in delayed matching tasks, and blockade of muscarinic cholinergic receptors also impairs performance in these tasks. Physiological data demonstrate that muscarinic cholinergic receptor stimulation activates intrinsic cellular currents in entorhinal neurons that could underlie the role of entorhinal cortex in performance of these tasks. Here we use a network biophysical simulation of the entorhinal cortex to demonstrate the potential role of this cellular mechanism in the behavioral tasks. Simulations demonstrate how the muscarinic-activated calcium-sensitive nonspecific cation current I_{NCM} could provide a cellular mechanism for features of the neuronal activity observed during performance of delayed matching tasks. In particular, I_{NCM} could underlie (1) the maintenance of sustained spiking activity during the delay period, (2) the enhancement of spiking activity during the matching period relative to the sample period, and (3) the resistance of sustained activity to distractors. Simulation of a larger entorhinal network with connectivity chosen randomly within constraints on number, distribution, and weight demonstrates appearance of other phenomena observed in unit recordings from awake animals, including match suppression, non-match enhancement, and non-match suppression.

Key words: delayed match to sample; delayed non-match; stellate cells; pyramidal cells; medial entorhinal cortex; afterhyperpolarization; working memory; biophysical modeling; computer simulation; nonspecific cationic current I_{NCM}

Lesions of the entorhinal and perirhinal cortices impair performance in delayed non-match to sample (DNMS) tasks in both non-human primates (Zola-Morgan et al., 1993; Leonard et al., 1995) and rats (Otto and Eichenbaum, 1992). In delayed non-match to sample tasks, stimuli are presented sequentially, and animals must respond to a particular stimulus if that stimulus does not match the previously presented stimulus. The role of the entorhinal cortex in these tasks may involve activation of muscarinic cholinergic receptors, because performance in delayed matching tasks is impaired by systemic injections of muscarinic cholinergic antagonists (Bartus and Johnson, 1976; Penetar and McDonough, 1983). Encoding of stimuli in a recognition memory task is impaired by local infusions of scopolamine into the perirhinal (and entorhinal) regions but not by infusions into the dentate gyrus or inferotemporal cortex (Tang et al., 1997), and microdialysis shows a 41% increase in acetylcholine levels in the perirhinal cortex during performance of this task (Tang and Aigner, 1996). Data from slice preparations of entorhinal cortex demonstrate a possible cellular mechanism for cholinergic modulation of entorhinal memory function. In physiological recordings from layer II principal cells in slice preparations (Klink and Alonso, 1997a,b), application of the cholinergic agonist carbachol causes long-term depolarizations, which have been termed plateau potentials. If neurons generate an action potential during cholinergic modulation, because of cholinergic depolarization or current injection, these neurons show sustained spiking activity. Modeling presented here demonstrates how plateau potentials and sustained spiking activity could arise from muscarinic cholinergic activation of a calcium-sensitive nonspecific cation current I_{NCM} for which *in vitro* physiological data have been obtained (Klink and Alonso, 1997a,b; Magistretti et al., 2001) (J. Magistretti, L. Ma, M. H. Shalinsky, and A. A. Alonso, unpublished observations). A current causing afterdepolarization also appears in prefrontal cortical neurons, but shows voltage dependence (Andrade, 1991; Haj-Dahmane and Andrade, 1996, 1998). Simplified models of short-term memory capacity have been inspired by these data (Lisman and Idiart, 1995; Jensen and Lisman, 1996, 1998).

The I_{NCM} could provide a potential mechanism for the selective maintenance of spiking activity in a subset of entorhinal cortical neurons for working memory function in behavioral tasks. Unit recording in awake behaving animals demonstrates specific patterns of spiking activity occurring during performance of delayed matching tasks (Suzuki et al., 1997; Young et al., 1997). These include stimulus-selective spiking activity during the delay period, enhancement of the spiking response to stimuli that match the previously presented sample stimulus, and resistance of sustained activity to distractors. Simulations presented here demonstrate how these phenomena could directly arise from I_{NCM} in individual entorhinal neurons. In addition, a number of studies have shown match suppression, in which spiking activity is weaker in response to a stimulus that matches the previously presented

Received April 4, 2001; revised Nov. 8, 2001; accepted Nov. 9, 2001.

This work was supported by National Institutes of Health Grants MH61492 and MH60013, by National Science Foundation Grant IBN9996177, and by a grant from the Human Frontier Science Program.

Correspondence should be addressed to Dr. Michael E. Hasselmo, Department of Psychology, Program in Neuroscience, and Center for Biodynamics, Boston University, 64 Cummington Street, Boston, MA 02215. E-mail: hasselmo@bu.edu.

 0270-6474/02/221081-17$15.00/0

sample (Suzuki et al., 1997; Young et al., 1997), as well as non-match enhancement and non-match suppression. Simulations of a large network with connectivity chosen randomly within constraints on number, distribution, and weight demonstrate how these additional phenomena can arise from network interactions of neurons with the intrinsic properties provided by the I_{NCM} current. This work has been published previously in abstract form (Fransén et al., 1999b, 2000).

MATERIALS AND METHODS

The GENESIS simulation package (Bower and Beeman, 1995) was used to model intrinsic properties of neurons in layer II of the entorhinal cortex. Separate compartmental biophysical simulations were developed for layer II stellate neurons, layer II pyramidal neurons, and layer II interneurons. The models used Hodgkin–Huxley representations of a range of intrinsic currents that underlie membrane potential changes in these neurons. The simulations presented here focus on how acetylcholine causes sustained depolarization and spiking activity in the pyramidal cells, and how these phenomena might underlie sustained activity and match enhancement during performance of delayed non-match to sample tasks (Young et al., 1997). Additional network simulations demonstrate that inclusion of inhibitory interneurons and inclusion of both stimulus-specific and nonspecific cells provides potential mechanisms for match suppression and non-match enhancement and suppression (Suzuki et al., 1997; Young et al., 1997).

Cell and network models

In these simulations, the entorhinal cortex layer II stellate and pyramidal cells (Klink and Alonso, 1997c) and interneurons (Jones and Buhl, 1993) have been reduced to equivalent cylinder models.

Entorhinal layer II pyramidal cells

The properties of entorhinal pyramidal cells were simulated with biophysical models containing multiple compartments, with an emphasis on the calcium-sensitive nonspecific cation current I_{NCM}. The compartmental structure of these simulations is shown in Figure 1. The pyramidal cell is composed of six compartments, one representing the soma, three representing the apical dendrite, one representing a basal dendrite, and one representing all but one basal dendrite lumped together, to constitute the main "load" to the soma. The proximal of the apical compartments, the basal dendrite, and the lump compartment are all connected to the soma. The lengths and cross sections of the three apical dendrite compartments were adjusted to give the dendrite a length constant of 2 (sealed-end condition). The compartment profiles are found in Table 1. Simulations with just a soma compartment and its conductances showed that dendritic compartments were not necessary to obtain robust spiking activity during delay periods in the cell. However, these dendritic compartments were important for matching a range of features in the data, including spike shape, afterhyperpolarization shape, and spike-frequency accommodation, as well as providing a more realistic attenuation of excitatory synaptic input.

Passive properties. Simulations of the passive membrane properties of the cell used the standard equivalent circuit representation for each compartment (Bower and Beeman, 1995).

The passive parameters are as follows: R_M, 5.0 Ωm^2; R_A, 1.0 Ωm; C_M, 0.01 F/m^2. The value of the membrane reversal potential E_m depends on contributions from leakage Na^+ and leakage Cl^- currents. (The K^+ leak current is explicitly represented as a separate current.) One may also view synaptic background activation with slow kinetics (e.g., NMDA and $GABA_B$) as part of the leakage current. Note that because the K^+ current is represented separately, its conductance should be added to the value of R_M given above when making comparisons with other data.

Active properties of pyramidal cells. The simulations included multiple currents underlying the active properties of the membrane, including both currents sensitive to changes in membrane potential and currents sensitive to intracellular calcium concentration. Equations describing the currents can be found in the section on ionic currents; the respective conductances are found in Table 4. The pyramidal cell model includes the following membrane currents listed in the section on ionic currents (with the appropriate subsection listed in parentheses): the Na^+ (Na) and K^+ (K_{dr}) currents responsible for fast action potentials, a high-threshold Ca^{2+} current (Ca_L), a calcium-dependent K^+ current (K_{AHP}), a fast calcium- and voltage-dependent K^+ current (K_C), a potassium leak current (K_{leak}), a persistent-type Na current (NaP), a noninactivating muscarinic K^+ current (K_M), and the muscarinic activated, nonspecific Ca^{2+}-sensitive cationic current I_{NCM} (NCM). The compartment where spikes are initiated (the soma in this case) has Na and K currents with faster kinetics [Na(soma) and K(soma)], based on previous work (Traub et al., 1994). In the experimental preparation, there are indications of a T-type Ca current (Bruehl and Wadman, 1999), but because these simulations result in relatively depolarized membrane potentials, this current was not included. To evaluate the ionic mechanisms of delay activity, additional simulations were performed with individual currents deleted.

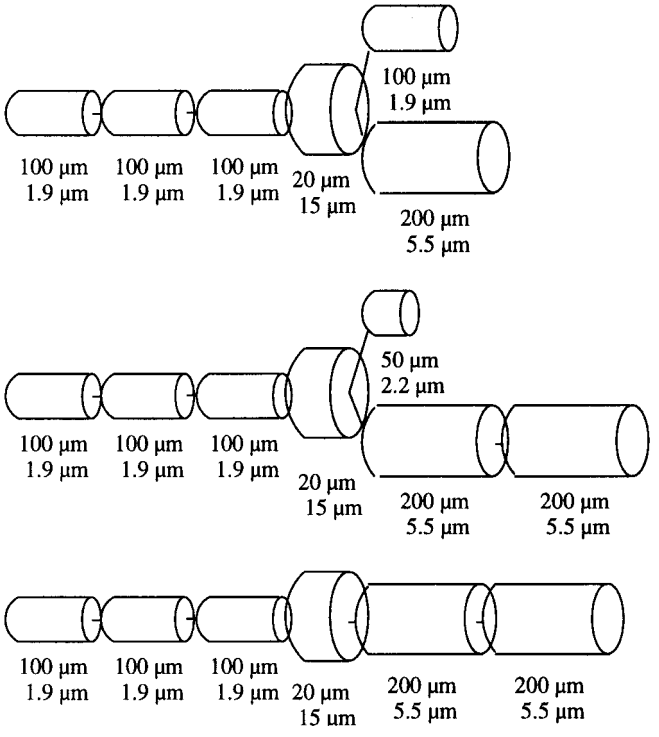

Figure 1. Schematic representation of the compartmental models used in the simulation of the intrinsic properties of entorhinal neurons, including pyramidal cells (*top*), stellate cells (*middle*), and interneurons (*bottom*). The dimensions of each component of the model are summarized in the figure.

Table 1. Compartment profile for the pyramidal cell

Compartment unit	Length (μm)	Diameter (μm)
Soma	20	15
Api. (×3)	100	1.9
Bas. (×1)	100	1.9
Lump (×1)	200	5.5

Api., Apical dendrite compartment; Bas., basal dendrite compartment.

Stellate cells

The properties of stellate cells were simulated with biophysical simulations containing multiple compartments. These simulations were developed for previous work on the mechanisms of subthreshold membrane potential oscillations in stellate cells (Fransén et al., 1998; Dickson et al., 2000) (E. Fransén, Alonso, and M. E. Hasselmo, unpublished observations). The compartmental structure of these simulations is shown in Figure 1. The stellate cell is composed of seven compartments. One compartment represents the soma; one compartment represents the initial segment; three compartments connected in succession represent the primary, secondary, and tertiary segments of a single principal dendrite; and two connected compartments represent all remaining den-

Table 2. Compartment profile for the stellate cell

Compartment unit	Length (μm)	Diameter (μm)
Soma	20	15
IS	50	2.2
Dendr. ($\times$3)	100	1.9
Lump ($\times$2)	200	5.5

IS, Initial segment compartment; Dendr., principal dendrite compartment.

Table 3. Compartment profile for the interneuron

Compartment unit	Length (μm)	Diameter (μm)
Soma	20	15
Dendr. ($\times$3)	100	1.9
Lump ($\times$2)	200	5.5

Dendr., Dendrite compartment.

drites lumped together. The addition of the separate initial segment compartment differs from the pyramidal cell. The lengths and cross sections of the three principal dendrite compartments were adjusted to give the dendrite a length constant of 2 (sealed-end condition). The compartment profiles are found in Table 2.

Passive properties. Simulations of the passive membrane properties of the cell used the same properties described above for pyramidal cells.

Active properties of stellate cells. Simulations of stellate cells included most of the same active currents included in the simulations of pyramidal cells, with adjustments in parameters to account for some of the differences in the intrinsic properties of these neurons. The K_{AHP} current is stronger in pyramidal cells than in stellate cells, and the K_M current is not present in stellate cells. As a consequence of the difference in conductance amplitudes, spike-frequency adaptation is stronger in pyramidal cells than in stellate cells. The stellate cells include a hyperpolarization-activated nonspecific cation current I_h that is not included in the pyramidal cell models. Equations describing the currents can be found in the section on ionic currents; the respective conductances are found in Table 5. The stellate cell model includes the following currents described in the section on ionic currents (with the appropriate subsection in parentheses): the Na^+ and K^+ currents responsible for fast action potentials (described in sections Na and K_{dr}), a high-threshold Ca^{2+} current (Ca_L), a calcium-dependent K^+ current (K_{AHP}), a fast calcium- and voltage-dependent K^+ current (K_C), a potassium leak current (K_{leak}), a persistent-type Na current (NaP), and a hyperpolarization-activated nonspecific cation current I_h (H).

Interneurons

The interneuron is modeled to replicate the basic properties of a fast-spiking nonadapting type cell. The interneuron is composed of six compartments, with one representing the soma, three representing a principal dendrite, and two representing all but one of the dendrites lumped together. The interneuron model does not have the separate initial segment compartment. The compartment profiles are found in Table 3.

Passive properties. Simulations of the passive membrane properties of the cell used the same properties described above for stellate cells.

Active properties. The interneuron model has the Na^+ and K^+ currents responsible for fast action potentials (Na and K_{dr}), a high-threshold Ca^{2+} current (Ca_L), a calcium-dependent K^+ current (K_{AHP}), and a potassium leak current (K_{leak}). The K_{AHP} was set at very weak values, consistent with the absence of spike-frequency accommodation in these neurons. The compartment where spikes are initiated (the soma in this case) has Na and K currents with faster kinetics [Na(soma) and K(soma)], as in previous models (Traub et al., 1994). Ionic conductances are found in Table 6.

Modeling of synaptic interactions

Synaptic currents in a postsynaptic neuron were activated by the membrane potential in the associated presynaptic neuron crossing a threshold value of -0.025 V. After a conductance delay of 2 msec, a synaptic current was initiated in the postsynaptic cell with a dual exponential time course (Bower and Beeman, 1995).

Synaptic contacts on the cells were either of a mixed AMPA/kainate and NMDA type or of a mixed $GABA_A$ and $GABA_B$ type. Equations describing the currents can be found in the section on synaptic currents; the respective parameters are found in Table 7.

The simulations included a conductance-based noise source. This represents potential effects of channel noise (White et al., 1998) or synaptic noise on actual neural function. The noise was generated from a Poisson process and was placed on the proximal lumped dendritic compartment.

Network models

The interaction of different cell types was analyzed in network simulations of different sizes. Many of the interactions of different cell types could be captured in small circuit simulations including six simulated neurons (see Fig. 6). These simulations included two neurons representing input to entorhinal cortex layer II, two simulated layer II pyramidal cells, one simulated layer II stellate cell, and one simulated layer II interneuron. One of the simulated pyramidal cells received input from only one input neuron, representing the odor-specific responses observed during unit recording (Young et al., 1997). The other simulated pyramidal cell received input from both input neurons, representing the odor nonspecific cells observed during recordings (Young et al., 1997). The input neurons did not contact the inhibitory interneuron, but the pyramidal cells, stellate cell, and interneuron were all interconnected with synaptic properties summarized in Table 7.

Larger-scale network simulations explored the interaction of larger numbers of neurons during several stages of a delayed matching task. They show how a single network of cells, with connectivity chosen randomly within constraints on number, distribution within a local neighborhood, and weight, can display many of the unit response types reported in experimental data (Suzuki et al., 1997; Young et al., 1997). See the section on network topology.

Computational methods

Biophysical simulations were developed using the GENESIS simulation package (Bower and Beeman, 1995). The Crank–Nicholson (Hines, 1984) method for numerical solution to differential equations was used (with modifications). A time step of 150 μsec was used for the simulations.

Ionic currents

Voltage-dependent conductances were modeled using a Hodgkin–Huxley type of kinetic model. The following reversal potentials were used: Na^+, +55 mV; K^+, -75 mV; Ca^{2+}, +80 mV; I_h, -20 mV; and I_{NCM}, 0 mV.

Na, K_{dr}. The Na^+ current responsible for fast action potentials had kinetics taken from a model of hippocampal pyramidal cells (Traub et al., 1991, 1994). The pyramidal cell and the interneuron have Na and K currents with faster kinetics [described in a separate section below and labeled Na(soma) and K_{dr}(soma)] on the compartment where spikes are initiated (Traub et al., 1994). Both the Na as well as the K current were shifted +5 mV from the model by Traub et al. (1991, 1994) to make the spiking threshold more positive (around -50 mV). The spatial distribution and maximal conductance of all currents on the different compartments are found in Tables 4–6. The maximal conductances were adjusted to match experimental data (Alonso and Klink, 1993) on the action potential rate of depolarization (Na^+) and rate of repolarization (K^+) as well as spike threshold, amplitude, and duration of action potentials. The currents used the following equations:

Na.

$$\alpha_m(V) = \frac{320 \times 10^3 (0.0131 - V)}{exp[(0.0131 - V)/0.004] - 1},$$

$$\beta_m(V) = \frac{280 \times 10^3 (V - 0.0401)}{exp[(V - 0.0401)/0.005] - 1},$$

$$\text{gate exponent} = 2;$$

$$\alpha_h(V) = 128 exp[(0.017 - V)/0.018],$$

$$\beta_h(V) = \frac{4 \times 10^3}{1 + exp[(0.040 - V)/0.005]},$$

$$\text{gate exponent} = 1.$$

Table 4. Conductance profile of the pyramidal cell

Current unit	Soma (S/m^2)	Prox. + med., api. + bas. (S/m^2)	Lump (S/m^2)	Dist. api. (S/m^2)
gNa	0	60	60	30
gK_{dr}	0	25	25	12
$gNaIS$	250	0	0	0
$gK_{dr}IS$	25	0	0	0
gK_C	1960	1960	1960	1960
gK_{AHP}	0.5	0.5	0.5	0.5
gCa_L	1.5	1.5	1.5	1.5
$gNaP$	2.0	0	0	0
gK_M	35	0	0	0
$gNCM$	26	0	0	0
gK_{leak}	1.0	1.0	1.0	1.0
$\phi Ca(K_C)pool$	61.34×10^{12}	38.85×10^{12}	16.73×10^{12}	38.85×10^{12}
$\phi Ca(K_{AHP})pool$	61.34×10^{12}	38.85×10^{12}	16.73×10^{12}	38.85×10^{12}
$\phi Ca(NCM)pool$	61.34×10^{12}	0	0	0

Maximal conductances (g) and calcium conversion factor (ϕ) for each compartment. For some of the currents, the density was assumed to be uniform. For the others, the general profile, with a higher conductance at the soma and gradually lower conductances for more distal dendritic compartments, was adopted from Traub et al. (1991). The criteria selected to adjust the conductances do not give a unique solution (Traub et al., 1991; DeSchutter and Bower, 1994). Prox., Proximal compartment; med., medial compartment; Dist., distal compartment; api., apical dendritic compartment; bas., basal dendritic compartment; lump, lumped dendritic compartment.

Table 5. Conductance profile of the stellate cell

Current unit	IS (S/m^2)	Soma (S/m^2)	Prox. + med. dendr. (S/m^2)	Prox. lump (S/m^2)	Dist. dendr. (S/m^2)	Dist. lump (S/m^2)
gNa	150	38	38	38	19	19
gK_{dr}	215	107	107	107	54	54
gK_C	0.0	13400	0.0	0.0	0.0	0.0
gK_{AHP}	0.0	0.1	0.1	0.1	0.1	0.1
gCa_L	0.0	1.0	1.0	1.0	1.0	1.0
$gH(fast)$	0.0	2.5	2.5	2.5	2.5	2.5
$gH(slow)$	0.0	1.2	1.2	1.2	1.2	1.2
$gNaP$	0.0	1.25	1.25	1.25	1.25	1.25
gK_{leak}	0.9	0.9	0.9	0.9	0.9	0.9
$\phi Ca(K_C)pool$	0.0	61.34×10^{12}	97.37×10^{12}	16.73×10^{12}	21.91×10^{12}	3.76×10^{12}
$\phi Ca(K_{AHP})pool$	0.0	61.34×10^{12}	97.37×10^{12}	16.73×10^{12}	21.91×10^{12}	3.76×10^{12}

Prox., Proximal compartment; med., medial compartment; Dist., distal compartment; dendr., principal dendritic compartment; lump, lumped dendritic compartment.

Table 6. Conductance profile of the interneuron

Current unit	Soma (S/m^2)	Prox. + med., dendr. + lump (S/m^2)	Dist. dendr. + dist. lump (S/m^2)
gNa	0	125	65
gK_{dr}	0	160	80
$gNaIS$	500	0	0
$gK_{dr}IS$	650	0	0
gK_{AHP}	1.0	0	0
gCa_L	1.0	0	0
gK_{leak}	0.2	0.2	0.2
$\phi Ca(K_{AHP})pool$	61.34×10^{12}	0	0

Prox., Proximal compartment; med., medial compartment; Dist., distal compartment; dendr., main dendritic compartment; lump, lumped dendritic compartment.

Na(*soma*).

$$\alpha_m(V) = \frac{800 \times 10^3(0.0172 - V)}{exp[(0.0172 - V)/0.004] - 1},$$

$$\beta_m(V) = \frac{700 \times 10^3(V - 0.0422)}{exp[(V - 0.0422)/0.005] - 1},$$

gate exponent = 3;

$$\alpha_h(V) = 320exp[(0.042 - V)/0.018],$$

$$\beta_h(V) = \frac{10 \times 10^3}{1 + exp[(0.042 - V)/0.005]},$$

gate exponent = 1.

K_{dr}.

$$\alpha_m(V) = \frac{16 \times 10^3(0.0351 - V)}{exp[(0.0351 - V)/0.005] - 1},$$

$$\beta_m(V) = 250exp[(0.020 - V)/0.040],$$

gate exponent = 2.

K_{dr}(*soma*).

$$\alpha_m(V) = \frac{30 \times 10^3(0.0172 - V)}{exp[(0.0172 - V)/0.005] - 1},$$

$$\beta_m(V) = 450exp[(0.012 - V)/0.040],$$

gate exponent = 4.

Ca_L. The high-threshold Ca^{2+} current was modeled according to

previous models (Traub et al., 1994). The maximal conductance was set to the same value as in previous work (Traub et al., 1994).

$$\alpha_m(V) = \frac{1.6 \times 10^3}{1 + exp[-72(V - 0.065)]},$$

$$\beta_m(V) = \frac{20 \times 10^3 (V - 0.0511)}{exp[(V - 0.0511)/0.005] - 1},$$

gate exponent = 2.

K_{AHP}. The calcium-dependent K^+ (afterhyperpolarization) current was modeled according to previous models (Traub et al., 1991), with the slope set at 30 and the saturation set at 30 (arbitrary units). The maximal conductance was adjusted to match the slow afterhyperpolarization (sAHP) depth in experimental data (Alonso and Klink, 1993).

$$\alpha_m([Ca^{2+}]) = min(30 \times [Ca^{2+}], 30),$$

$$\beta_m = 1.0,$$

gate exponent = 1.

K_C. The fast calcium- and voltage-dependent K^+ current was modeled according to previous work (Traub et al., 1991). The maximal conductance was adjusted to match the fast afterhyperpolarization (fAHP) depth and Ca-dependent spike repolarization rate (Alonso and Klink, 1993).

$$V \leq 0.050,$$

$$\alpha_m(V) = \frac{exp(53.872V - 0.66835)}{0.018975},$$

$$\beta_m(V) = 2000[exp([0.0065 - V]/0.027)] - \alpha_m;$$

$$V > 0.050,$$

$$\alpha_m(V) = 2000[exp([0.0065 - V]/0.027)],$$

$$\beta_m(V) = 0,$$

gate exponent = 1.

K_M. The slowly activated voltage-dependent K^+ current was modeled according to Bhalla and Bower (1993). The maximal conductance was adjusted to match the length of the suprathreshold plateau after a spike in the presence of a Ca block (Alonso and Klink, 1993).

$$\tau_m(V) = \frac{1}{3.3\ exp[(V + 0.035)/0.040] + exp[-(V + 0.035)/0.020]},$$

$$m_{inf}(V) = \frac{1}{1 + exp[-(V + 0.035)/0.005]},$$

gate exponent = 1.

H. The hyperpolarization-activated nonspecific cation current I_h was modeled according to previous work (Dickson et al., 2000) (Fransén Alonso, and Hasselmo, unpublished observations). The maximal conductance was adjusted to comply with voltage-clamp data as well as current-clamp data on the "sag" produced by I_h (Dickson et al., 2000).

$$\tau_m(fast)(V) = \frac{0.00051}{exp[(V - 0.0017)/0.010] + exp[-(V + 0.34)/0.052]},$$

$$m_{inf(fast)}(V) = \frac{1}{[1 + exp[V + 0.0742]/0.00978)]^{1.36}},$$

gate exponent = 1;

$$\tau_m(slow)(V) = \frac{0.0056}{exp[(V - 0.017)/0.014] + exp[-(V + 0.26)/0.043]},$$

$$m_{inf(slow)}(V) = \frac{1}{[1 + exp([V + 0.00283]/0.0159)]^{58.5}},$$

gate exponent = 1.

NaP. The persistent-type slowly inactivating Na^+ current was modeled according to experimental data (Magistretti et al., 1999) for the steady-state activation and inactivation and kinetics of inactivation and for the reversal potential, and according to McCormick and Huguenard (1992) for the kinetics of activation and the exponents of the activation rates m and h. The maximal conductance was adjusted to the conductance of I_h to allow subthreshold oscillations to develop.

$$\tau_m(V) = \frac{1}{\alpha_m + \beta_m}, \text{ where } \alpha_m(V) = \frac{0.091 \times 10^6 (V + 0.038)}{1 - exp[-(V + 0.038)/0.005]}$$

$$\text{and} \quad \beta_m(V) = \frac{-0.062 \times 10^6 (V + 0.038)}{1 - exp[(V + 0.038)/0.005]},$$

$$m_{inf}(V) = \frac{1}{1 + exp[-(V + 0.0487)/0.0044]},$$

gate exponent = 1;

$$\tau_h(V) = \frac{1}{\alpha_h + \beta_h}, \quad \text{where } \alpha_h(V) = \frac{-2.88V - 0.0491}{1 - exp[(V - 0.0491)/0.00463]}$$

$$\text{and} \quad \beta_h(V) = \frac{6.94V + 0.447}{1 - exp[-(V + 0.447)/0.00263]},$$

$$h_{inf}(V) = \frac{1}{1 + exp[(V + 0.0488)/0.00998]},$$

gate exponent = 1.

K_{leak}. The K_{leak} conductance was considered to be linear and uniformly distributed with a reversal potential of: $E_{rev} = -0.075\ V$.

NCM. The nonspecific Ca^{2+}-dependent cationic current was modeled using a framework similar to the calcium-dependent K^+ current found in previous work (Traub et al., 1991). Time constants for the I_{NCM} were derived by replicating experimental data (Klink and Alonso, 1997a,b). Note that these experimental data were fitted by modifying the total kinetics of both the calcium diffusion and the I_{NCM} current to replicate experimental traces.

Here we focus on the Ca-sensitive component of I_{NCM}. Recent evidence suggests that I_{NCM} also has a calcium-insensitive component, but this is not explicitly modeled in our simulations. The resting potential of our simulations, before any input has been presented, corresponds to a resting state with cholinergic modulation that would include conductance contributions attributable to the calcium-insensitive component. The maximal conductance was adjusted to produce spiking frequencies similar to those observed during delay activity and during match enhancement in recordings of single units in awake rats performing a delayed non-match to sample task (Young et al., 1997).

$$\alpha_m([Ca^{2+}]) = min(0.02 \times [Ca^{2+}], 10),$$

$$\beta_m = 1.0,$$

gate exponent = 1.

Ca^{2+} buffering

The Ca^{2+} diffusion and buffering was modeled according to previous techniques (Traub et al., 1991; McCormick and Huguenard, 1992). To take into account the differences in distances and diffusion constants for the calcium influencing each of the different currents, the calcium kinetics was modeled separately for each case, consistent with separate calcium compartments and reaction pathways within the cell. In addition, until calcium-clamp data exist on the individual currents, it is not possible to separate the kinetics of the calcium concentration from the kinetics of the channel itself. Therefore, the models of the concentration and of the individual currents should be seen as a unit.

Table 7. Synaptic parameters

Compartment unit	E_{rev} (V)	τ_r (sec)	τ_d (sec)
AMPA	0	0.002	0.002
NMDA	0	0.08	0.00067
$GABA_A$	−0.070	0.001	0.007
$GABA_B$	−0.085	0.03	0.09

Following the convention used in Traub et al. (1991), the calcium concentration has arbitrary units. Because the calcium concentration is converted to an effect on rate parameters of the calcium-sensitive channel, the absolute concentration of calcium can be arbitrary, although we have tried to keep the magnitude in a range similar to millimolar to enable comparisons. For the calcium related to the calcium-dependent K^+ current, the diffusion rate constant of 0.1 sec was set to give a spike-frequency adaptation rate according to Alonso and Klink (1993). The minimal $[Ca^{2+}]_i$ was set to 5.0×10^{-3}.

For the fast calcium- and voltage-dependent K^+ current (K_C), the calcium values were 0.5 msec and 5.0×10^{-6}, respectively, and the related values for the non-specific Ca^{2+}-dependent cationic current were 1.333 sec and 1.0×10^{-5}, respectively. This was determined by tuning the channel to replicate data obtained during blockade of calcium influx by Klink and Alonso (1993). The changes in the concentration of calcium used for K_{AHP} above were too slow to effectively represent K_C, so different dynamics were necessary. Similarly, the slower changes in I_{NCM} relative to K_{AHP} required use of the slower calcium dynamics for I_{NCM} described above. In addition, the conversion factor, ϕ, from charge density to concentration for each component and compartment is found in Tables 4–6. Because this conversion factor converts channel current to calcium concentration, valence is implicitly addressed by using current.

Synaptic currents

Synaptic conductances between neurons were modeled with an α function (Bower and Beeman, 1995): $g_{syn} = (A \times g_{max})/(\tau_d - \tau_r)\ (e^{-t/\tau_d} - e^{-t/\tau_r})$, where g_{max} is the peak synaptic conductance, τ_r is the rising time constant, τ_d is the decaying time constant, g_{syn} is the synaptic conductance at time t, and A is a scaling constant set to yield a maximum conductance of g_{max}.

For the NMDA current, the conductance was multiplied with the magnesium block conductance described previously (Zador et al., 1990): $g_{Mg} = 1/(1 + 0.018e^{-60\,V})$.

Before determining the synaptic conductance values, the relative proportions of the various components were fixed according to the following experimental data: The NMDA component has the same postsynaptic potential (PSP) height as AMPA at −72 mV (Alonso et al., 1990). $GABA_A$ is 70% of $GABA_B$ at −66 mV (Gloveli et al., 1999).

The synaptic conductances were adjusted so that firing rates would resemble those observed in recordings of entorhinal units from rats performing a delayed non-match to sample task (Young et al., 1997) for the various parts of an experiment (i.e., sample, delay, and test). Note that firing rates were matched to firing rates observed in rats, but for phenomena of match as well as non-match enhancement and non-match suppression, the relative changes in firing rates were adjusted to match those observed in monkeys (Suzuki et al., 1997). The values of τ_r and τ_d can be found in Table 7. The values of g_{max} can be found in Tables 8–11.

Network topology

Smaller example networks were used to illustrate the fundamental features of connectivity that could result in specific phenomena observed in unit recordings of entorhinal neurons during delayed matching tasks. These simple example networks used the basic connectivity summarized in Figure 6, with synaptic conductances found in Tables 8–10. Table 8 shows the synaptic conductances for Figure 7, Table 9 shows conductances for Figures 8 and 9*A*, and Table 10 shows conductances for Figure 9*B*.

To demonstrate that these simple interactions could easily be obtained with connectivity chosen randomly within constraints on number, distribution, and weight, a larger network simulation was developed. As shown in Figure 10, the larger network consists of one population of 12 input cells representing association cortices projecting into the entorhinal cortex, one population of 30 stellate cells, one population of 18 pyramidal cells, and one population of 12 interneurons. The relative proportion of EC cells was determined according to experimental findings (Alonso and Klink, 1993), although these estimates may be subject to differences in the probability of sampling different types of neurons.

Table 8. Pure delay activity and match enhancement

Pre-cell	Stim A	Stim B	Stel	Pyr A	Pyr AB	Int
Post-cell						
Stel				0.1029		2.237
Pyr A	0.5761					3.356
Pyr AB	0.5761	0.5761				1.678
Int			0.1409	0.1409	0.2058	

Stim A, Input to cell A; Stim B, input to cell B; Stel, stellate cell; Pyr, pyramidal cell; Int, interneuron. Values refer to AMPA or $GABA_A$ conductances. The values for NMDA or $GABA_B$ conductances are scaled with a factor of 3 and 0.16, respectively. Synaptic conductances are in 10^{-9} S.

Table 9. Match suppression and non-match enhancement

Pre-cell	Stim A	Stim B	Stel	Pyr A	Pyr AB	Int
Post-cell						
Stel	0.05144	0.05144			0.1080	0.4474
Pyr A	0.5761					2.237
Pyr AB	0.5761	0.5761				2.237
Int			0.09014	0.2113		

Stim A, Input to cell A; Stim B, input to cell B; Stel, stellate cell; Pyr, pyramidal cell; Int, interneuron. Values refer to AMPA or $GABA_A$ conductances. The values for NMDA or $GABA_B$ conductances are scaled with a factor of 3 and 0.16, respectively. Synaptic conductances are in 10^{-9} S.

The input cells were divided into three equal groups representing three stimuli (*A*, *B*, and *C*). *A* did not overlap at all with *B* or *C*, but *B* and *C* had moderate overlap. The existence of a connection was determined randomly within a window of possible connections. The connection strengths from one of the inputs to either the stellates or the pyramidal cells had a uniform value for a central set of connections and decreasing values for neurons at the sides of the central projection, to provide fully activated cells as well as weakly activated cells. The input cells contacted both stellates and pyramidal cells.

The stellate cells, pyramidal cells, and interneurons connected to the other cell types according to a localized scheme. Geometrically, each population was uniformly spaced on a line of unit length. A pair of presynaptic and postsynaptic cells from two cell populations corresponded if they occupied the same position within the line. A presynaptic cell was first randomly selected and a postsynaptic cell was thereafter randomly selected within a window centered around the corresponding cell in the postsynaptic type. The resulting percentage of connectivity between individual populations of cell types is shown in Figure 10, and the total number of connections between different populations is shown in Table 12. Additionally, as a control, the number of connections, window width, and conductance values were varied to test the sensitivity of the model.

RESULTS

Single-cell mechanisms for sustained spiking activity

The compartmental biophysical models of entorhinal layer II pyramidal cells were used to simulate intracellular recording data from this type of cell obtained in brain slice preparations of the entorhinal cortex (Alonso and Klink, 1993; Klink and Alonso, 1993). The parameters of the intrinsic currents listed in Materials and Methods were adjusted to simulate specific examples of the intrinsic properties observed during these intracellular recordings. As shown in Figure 2, simulations were tuned to replicate the properties of spike shape and spike-frequency accommodation observed in the experimental data in the absence of cholinergic modulation. This figure follows the same time course for

Table 10. Non-match suppression

Pre-cell	Stim A	Stim B	Stel	Pyr A	Pyr AB	Int
Post-cell						
Stel	0.05144	0.05144		0.1800		0.4474
Pyr A	0.5761					2.237
Pyr AB	0.5761	0.5761				2.237
Int			0.09014		0.2113	

Stim A, Input to cell A; Stim B, input to cell B; Stel, stellate cell; Pyr, pyramidal cell; Int, interneuron. Values refer to AMPA or $GABA_A$ conductances. The values for NMDA or $GABA_B$ conductances are scaled with a factor of 3 and 0.16, respectively. Synaptic conductances are in 10^{-9} S.

Table 11. Larger network

Pre-cell	Stim	Stel	Pyr	Int
Post-cell				
Stel	0.05144		0.06430	2.461
Pyr	0.2469	0.05144		2.461
Int		0.05066	0.1187	

These values are used for the AMPA and $GABA_A$ conductances. The values for NMDA or $GABA_B$ conductances are scaled with a factor of 3 and 0.16, respectively. Synaptic conductances are in 10^{-9} S.

stimulation that is shown in Figure 10*A* of Alonso and Klink (1993).

In physiological recordings from pyramidal cells in brain slice preparations (Klink and Alonso, 1997a,b), application of the cholinergic agonist carbachol causes long-term depolarizations, which have been termed plateau potentials. These plateau potentials appear to arise from muscarinic receptor activation of a nonspecific cation current I_{NCM} (Magistretti, MA, Shalinsky, and Alonso, unpublished observations). This nonspecific cation current has a sensitivity to intracellular calcium concentration changes caused by calcium influx through voltage-gated calcium channels (Ca_L) (Magistretti et al., 2001). Experimental data show that the muscarinic-activated, calcium-sensitive, nonspecific cation currents have the potential to cause sustained repetitive spiking activity in single neurons (Klink and Alonso, 1997b). The combined cholinergic muscarinic receptor activation of the I_{NCM} current and block of potassium currents I_{KAHP} and I_{KM} brings the cell closer to its firing threshold. If the neuron then discharges, the spike-associated calcium influx potentiates I_{NCM}, leading to additional depolarization. The spiking necessary to induce sustained firing can also be induced by synaptic input or current injection.

As shown in Figure 3, computational modeling of this current demonstrates potential mechanisms for the generation of sustained spiking activity in single neurons. The self-sustained generation of spiking activity results from the following cycle: (1) each action potential causes an influx of calcium through voltage-sensitive calcium channels; (2) the inflow of calcium replenishes the pool of calcium acting to enhance the activity of the calcium-sensitive I_{NCM} current; and (3) the sustained activation of the I_{NCM} current depolarizes the cell sufficiently to cause generation of another action potential, thereby repeating the cycle.

Delay activity and match enhancement

This intrinsic cellular mechanism could underlie certain aspects of the neuronal firing activity observed in the entorhinal cortex during performance of a continuous DNMS (cDNMS) task with odors in rats (Young et al., 1997). In particular, the cellular

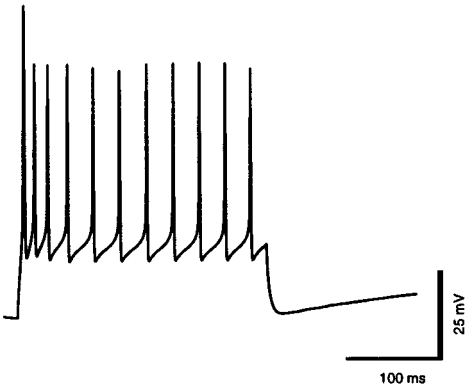

Figure 2. Spike-frequency accommodation in a simulated layer II pyramidal cell during membrane depolarization in response to a 265 msec simulated current injection. This cell contains a wide range of voltage- and calcium-dependent currents. The figure displays the response properties of the neuron in the absence of cholinergic modulation.

mechanism in single neurons could account for the spiking phenomena observed during the performance of these tasks, including (1) delay activity, and (2) match enhancement (Young et al., 1997). The term delay activity refers to the stimulus-selective activity induced by a sample stimulus that can be maintained after the stimulus ends and throughout the delay period until the next stimulus is presented. The term match enhancement refers to trials in which an individual neuron generates more spikes in response to a test stimulus that matches the preceding sample stimulus than were generated in response to the same test stimulus when it did not match the preceding sample stimulus.

Cholinergic modulation of I_{NCM} could provide a mechanism for stimulus-selective delay activity and match enhancement. If there is an increase in acetylcholine levels during performance of the task, then the spiking activity induced in a set of neurons by a specific sensory stimulus (i.e., a single odor) can be maintained because of the repetitive activation mechanism described above, as shown in Figure 3. In these simulations, we replicated the time course of different components of the behavioral cDNMS task used during *in vivo* unit recordings from the entorhinal cortex (Young et al., 1997). The task is simulated with a 600 msec current injection representing afferent input to the entorhinal cortex during sniffing of one odor during the stimulus period of the task, followed by a 2400 msec delay period with no current injection, and followed by a 600 msec current injection representing afferent input to the entorhinal cortex during sniffing of the same odor during the next stimulus period (corresponding to a match condition). (Fig. 3*D* illustrates the timing of current injection.)

The trace in Figure 3*A* shows how a neuron responds after simulated cholinergic activation of the I_{NCM} current. A suprathreshold input causes spiking during the stimulus period, which causes calcium influx through voltage-sensitive calcium channels. This calcium influx causes additional activation of the calcium-sensitive I_{NCM} current, which depolarizes the membrane sufficiently to cause another action potential even after the end of the depolarizing current injection. Each subsequent spike causes sufficient depolarization to induce another spike, allowing self-sustained spiking activity throughout the delay period until the next stimulus is given. When the second presentation of the same stimulus occurs, the cell is already depolarized by I_{NCM} activation, such that it responds to the "match" stimulus with consid-

erably greater spiking than the initial response to that same stimulus. A comparison of this match period with the preceding stimulus period corresponds to the match enhancement observed previously (Young et al., 1997). Thus, I_{NCM} provides an intrinsic mechanism appropriate for both the sustained delay activity and the match enhancement phenomenon. Between the spiking activity produced by the current injection and the spikes produced by the I_{NCM} depolarization, there may be an interval without spikes. This interval also appears before sustained spiking in experimental data from brain slice preparations, as seen in Figure 5*A*.

The top example in Figure 3*A* shows match enhancement after delay activity, but neurophysiological studies indicate that many neurons show match enhancement even without delay activity (Young et al., 1997). The trace in Figure 3*B* shows that match enhancement can be observed in the simulation even in the absence of sustained delay activity. This could provide another neurobiological mechanism for performing matching that does not depend on maintaining activity during the delay. In this example, the spiking activity during the initial depolarization does not cause sufficient activation of I_{NCM} to induce additional spiking after the end of the initial afferent input. However, the subthreshold depolarization attributable to I_{NCM} persists during the delay period, causing enough residual depolarization that a new afferent input at the end of the delay period causes generation of a larger number of spikes. Thus, match enhancement can occur without delay activity. This subthreshold depolarization decays with a time constant of 3.6 sec, which is sufficiently slow enough to mediate match enhancement after a 3 sec interval. This suggests that match enhancement after longer delays without spiking results from input from neurons showing persistent activity or from longer-term synaptic changes. Figure 3*B* may be compared with *in vitro* experimental data in Figure 5*B* showing stronger responses to a second identical current injection even when there is no delay activity. The trace in Figure 3*C* shows what happens without cholinergic enhancement of I_{NCM}. In this case, the neuron will spike during the initial stimulus period, but the absence of I_{NCM} activation prevents the neuron from showing sustained depolarization and spike generation during the delay period. In addition, the absence of a depolarization during the delay prevents the neuron from generating increased spiking activity during the match stimulus. Thus, it fires the same number of spikes in response to the match stimulus that it did in response to the previous input. In this framework, cholinergic activation of the calcium-sensitive I_{NCM} is important to the intrinsic mechanisms for sustained activity and match enhancement. This is consistent with data showing that muscarinic cholinergic antagonists cause impairments of behavioral performance in delayed match to sample tasks (Bartus and Johnson, 1976; Penetar and McDonough, 1983; Tang et al., 1997).

The simulation in Figure 3*A* shows acceleration of the firing rate attributable to the internal buildup of calcium, which causes a persistent increase in firing rate. This acceleration can be avoided by having the I_{NCM} current in the range of saturation, so that additional depolarization does not cause additional activation of the current. This causes a stable rate of firing to be obtained more rapidly during the delay period, as shown in Figure 3*E*. This acceleration of the firing rate can also be prevented by network interactions. For example, feedback inhibition in the network allows initial acceleration during the delay period to reach an asymptotically stable firing frequency at the end of the delay, as shown in Figure 3*F*. In this example, even the addition of a single interneuron mediating feedback inhibition can prevent

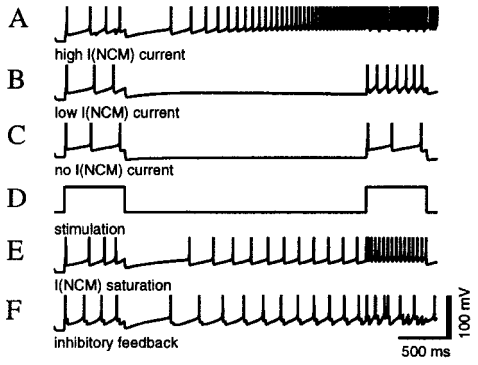

Figure 3. Simulation of delay activity and match enhancement in a pyramidal cell during a delayed matching task attributable to cholinergic enhancement of the I_{NCM} current. Traces show responses to two 600 msec current injections with a 2400 msec delay between injection. *A*, Generation of sustained spiking activity during the delay period. At the start of the simulation, muscarinic activation of the I_{NCM} current causes subthreshold activation. During an initial 600 msec current injection, spike generation causes an influx of calcium through voltage-sensitive calcium channels. This calcium influx activates the calcium-sensitive I_{NCM}, causing generation of an additional spike well after the end of the current injection. This causes additional calcium influx which causes additional I_{NCM} activation and additional depolarization, resulting in sustained spiking behavior. The response to a subsequent 600 msec current injection shows considerably greater spiking activity than the response to the first current injection. *B*, Generation of match enhancement. Even without spiking during the delay period, the activation of the I_{NCM} by the initial spiking activity persists long enough that a residual depolarization at the end of the delay period results in greater spiking activity during the second current injection. *C*, Without cholinergic activation of I_{NCM} the response of the cell is similar during the two current injection periods. *D*, Timing of current injection during sample and test periods. *E*, Sustained spiking during the delay period with I_{NCM} in the range of saturation, which causes acceleration to asymptotically approach a lower stable firing rate. *F*, Interaction of the simulated pyramidal cell from *A* with feedback inhibition also allows a stable firing frequency during sustained spiking activity. In this simple example, a single inhibitory interneuron responds to pyramidal cell spiking activity and causes feedback inhibition that maintains spiking activity at a moderate frequency during the delay period. (At the end of the delay, the neuron still shows match enhancement in response to the second current injection.)

the simulated pyramidal cell in Figure 3*F* from showing continuous acceleration of the firing rate. The neuron reaches a stable firing rate during the delay period but still shows match enhancement during the second current injection relative to the sample stimulus. Delay activity of this sort can be obtained in experiments with concentrations of carbachol as low as 2 μM, which is comparable with the range of physiologically realistic endogenous concentrations of acetylcholine. In experiments in layer V, delay activity of this sort can be induced by stimulation of synaptic input as well as direct current injection. Figure 3, *E* and *F*, may be compared with *in vitro* data in Figure 5*A* showing sustained spiking after current injection.

Additional simulations were performed to further evaluate the role of I_{NCM} in this delay activity. In particular, we found no change in delay activity after individual removal of either the *NaP* current or K_M. (In these simulations, the resting potential was kept the same with a 0.04 nA current injection after deleting *NaP* and with a −0.02 nA current injection after deleting K_M.) The delay activity could also be maintained after combined deletion of *NaP*, K_M, Ca, and K_{AHP} from the simulation. (For the calcium current, the charge flow was removed from the calculation, but the

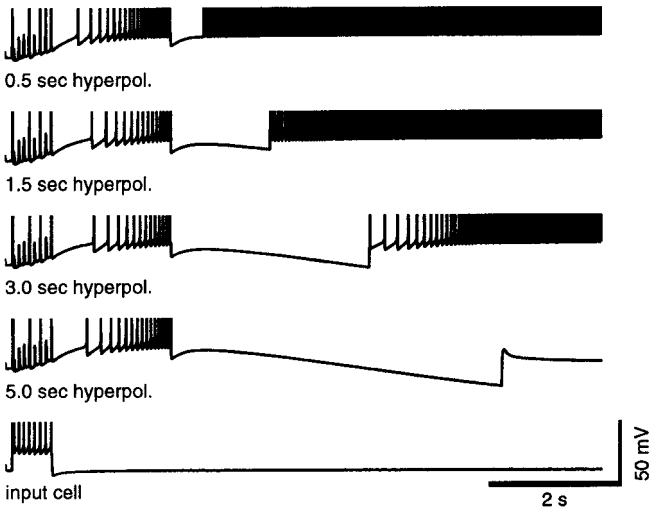

Figure 4. Sustained activity can resist periods of hyperpolarization, suggesting that this mechanism of working memory can resist moderate interference. These simulations show the membrane potential during simulation of muscarinic enhancement of the I_{NCM}. In each trace, synaptic input from the cell at the *bottom* causes generation of a series of spikes (action potentials are truncated to ease viewing of subthreshold membrane potential changes). After the EPSPs have ended, the membrane potential continues to rise due to activation of I_{NCM}, resulting in sustained spiking activity. In each of the *top four traces*, hyperpolarizing current injections of different durations are simulated. In the first three durations, spiking activity is terminated during hyperpolarization but commences again after hyperpolarization has ended. This is possible because of the lack of voltage dependence of I_{NCM}. Only when hyperpolarization persists for 3–4 sec does sustained spiking activity terminate. The *bottom trace* shows the activity of the input cell.

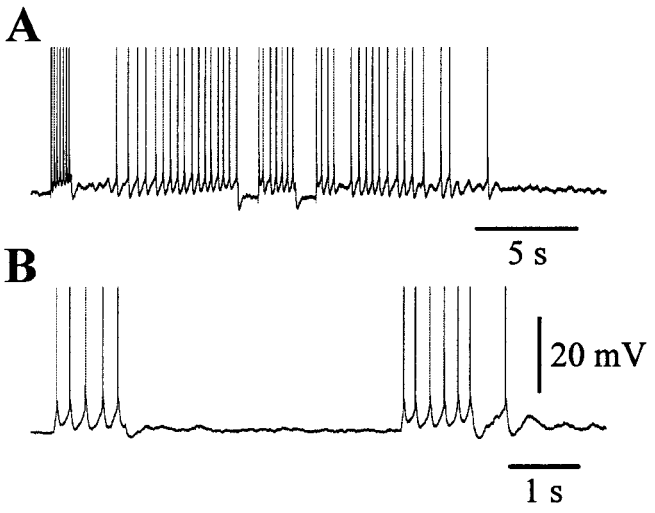

Figure 5. Experimental data showing examples of sustained spiking activity and match enhancement during whole-cell patch recording in slice preparations of entorhinal cortex. Recordings were performed in standard Ringer's solution with 100 μM picrotoxin and 1 mM kynurenic acid added to block synaptic transmission. The cholinergic agonist carbachol was present in a concentration of 20 μM. *A*, Sustained spiking activity after current injection. In the presence of carbachol, spiking induced by a short current injection is followed by sustained spiking activity after a brief interval. This spiking activity accelerates and persists despite two hyperpolarizing pulses presented at the *middle* of the *trace*. The amplitude of the current pulses was −50 pA. *B*, Match enhancement without delay activity. Because of cholinergic activation of the I_{NCM}, the neuron fires more spikes in response to the second repetition of the same current injection, despite the absence of spiking during the delay. The amplitude of the current pulses is 40 pA.

flow of calcium to the calcium concentration was kept so that all calcium-dependent currents would remain unaffected.) Note that evaluation of the sustained spiking activity requires that the cell still generate normal action potentials, which required retention of the *Na*, K_{dr}, and K_C currents. K_{leak} was retained to maintain resting potential. The importance of the *NCM* current was also demonstrated by showing in an otherwise intact simulation that a reduction of I_{NCM} by 27% prevented any delay activity. (In this simulation, resting potential was maintained with a depolarizing current injection of 0.016 nA.)

The intrinsic mechanism of I_{NCM} for generation of sustained spiking activity appears to be resistant to brief periods of interference, which could cause inhibitory input to the neurons in the network. This is consistent with the fact that delay activity can sometimes persist through presentation of intervening stimuli in a delayed matching to sample (DMS) task (Suzuki et al., 1997). As shown in Figure 4, the neurons are resistant to a range of short duration hyperpolarizing current injections. Only after the current injection exceeds a 3–4 sec duration does the neuron terminate the sustained spiking activity. Figure 4 (*top*, *left* and *right*) may be compared with *in vitro* experimental data in Figure 5*A* showing resistance of sustained spiking to hyperpolarizing current injections. This resistance to hyperpolarization arises from the lack of voltage dependence of I_{NCM}. The length of the resistance to hyperpolarization depends upon the conductance of I_{NCM}. At the values shown in Figure 4, the delay activity survives a 3 sec hyperpolarization but not a 3.5 sec hyperpolarization. With a 5% decrease in *NCM* conductance, the delay activity withstands 2 sec but not 2.5 sec of hyperpolarization. With a 10% increase, the delay activity withstands 4 sec but not 4.5 sec of hyperpolarization. A dominant effect of distractor stimuli during delayed matching might be depolarization of neurons within the network. Therefore, we also tested the effect of a 0.5 nA depolarizing current injection. Spiking rate was increased during the injection, but delay activity persisted after depolarizing injections of any duration. Experimental data from slice preparations also shows that depolarizing current injections do not terminate sustained spiking activity (Alonso, unpublished observations).

Match enhancement and delay activity in experimental data

The simulations described above were primarily developed to replicate *in vivo* data on match enhancement and delay activity. However, as noted above they can also be compared with available data on such phenomena observed during whole-cell patch recording in brain slice preparations of the entorhinal cortex, as shown in Figure 5. Figure 5*A* shows an example of persistent spiking activity appearing after a current injection. This trace also shows that the sustained spiking activity is not terminated by hyperpolarizing current injections. Figure 5*B* shows that even without delay activity, the recorded neuron shows a stronger spiking response to the second of two identical current injections.

Examples of network mechanisms for neuronal activity during delayed matching tasks

The intrinsic activation of I_{NCM} described in the previous section cannot account for all of the phenomena observed during unit recording in delayed non-match to sample and delayed match to sample tasks. For example, the spiking activity observed in these

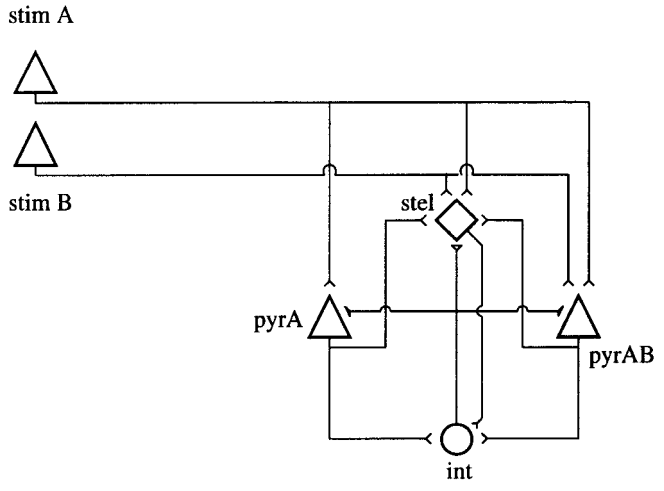

Figure 6. Connectivity of the minimal network simulation. The network represents layer II of the medial entorhinal cortex. In this layer, the principal cells are stellate cells and pyramidal cells together with an interneuron-type cell, as found in the rat (Alonso and Klink, 1993) and in the primate (P. Buckmaster, D. Amaral, and Alonso, unpublished data). This diagram shows the principal connectivity, but not all connections are present in all simulated networks. The network receives synaptic connections from input cells (*stim A* and *stim B*). The network contains two simulated pyramidal cells, including one representing cells with stimulus selectivity (*pyr A*, which receives afferent input only from *stim A*) and one representing cells with nonspecific responses (*pyr AB*, which receives afferent input from both *stim A* and *stim B*). The network also contains a stellate cell (*stel*), which receives input from *stim A* and *stim B* and from both pyramidal cells. The pyramidal cells connect with one another and with the inhibitory interneuron (*int*), which sends inhibitory connections to all neurons. In the larger model (Fig. 10), the number of stellate cells is larger than the number of pyramidal cells, as found in experimental data; here the network represents a minimal set of cell types to exemplify various cell types that have been classified in the literature according to their firing characteristic. Connection strengths for individual examples are summarized in Tables 8–10.

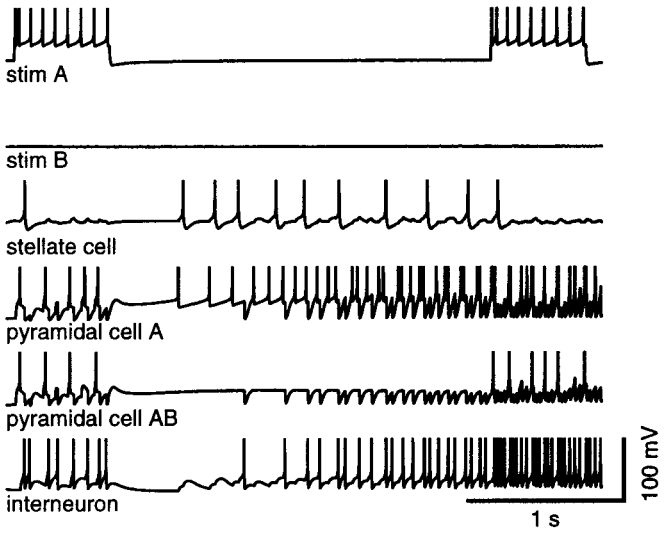

Figure 7. Delay activity in the network simulation. The simulated membrane potential is plotted for a 3.8 sec period for six different neurons: Input neurons stim A and stim B, a stellate cell, pyramidal cells A and AB, and an inhibitory interneuron. For a match trial, input cell stim A is activated during a 600 msec sample period, providing excitatory afferent input to both pyramidal cell A and pyramidal cell AB. This input is sufficient to cause pyramidal cell A to show sustained spiking during the 2.4 sec delay period, because of the regenerative activity of I_{NCM}. This spiking activity drives spiking in the stellate cell and interneuron. Stim A is activated again during the matching period, resulting in match enhancement. Action potentials are truncated in this figure. Synaptic conductances are summarized in Table 8.

experiments shows phenomena such as match suppression as well as non-match enhancement and non-match suppression. However, simple network interactions could underlie these additional spiking phenomena. We have tested potential mechanisms in small example networks, as shown in this section. Although these effects have been selectively tuned in these small networks, they can appear in a larger network with connectivity chosen randomly within constraints on number, distribution, and weight (see below).

As described in Materials and Methods and illustrated in Figure 6, the small example networks contain two input neurons (stim A and stim B), a selective pyramidal cell that receives input only from stim A (pyramidal cell A), a nonselective pyramidal cell that receives input from both stim A and stim B (pyramidal cell AB), a stellate cell, and an interneuron. Thus, these simulations include the experimental finding that some cells show stimulus specificity, whereas others do not. For simplicity, no cells showing specificity to stim B are shown.

Figure 7 demonstrates how delay activity can appear in a selective subset of neurons for a specific input pattern. The network receives afferent input from input neuron A, which more strongly activates pyramidal cell A. The spiking activity in pyramidal cell A is sufficient to result in regenerative activity during the delay period in this neuron, but not in a neuron that received slightly less afferent input (pyramidal cell AB). Note that excitatory synaptic transmission attributable to regenerative spiking activity in pyramidal cell A also drives spiking during the delay period in the stellate cell and in the interneuron. Thus, synaptic connectivity can cause delay activity in neurons that have no intrinsic mechanisms for that delay activity. Note also that the activity in the stellate cell only appears during the delay period, and not during the sample or test periods. The presence of I_{NCM} in a subset of neurons can drive network activity even if the synaptic connectivity alone would not allow sustained spiking activity. The synaptic conductances for this simulation are shown in Table 8.

Match suppression

In addition to the match enhancement described above, many researchers have described suppression of the response to the second viewing of a particular stimulus in the entorhinal cortex (Fahy et al., 1993; Suzuki et al., 1997; Young et al., 1997) and inferotemporal cortex (Miller and Desimone, 1993, 1994). In most studies, both match enhancement and match suppression are reported, but studies have often focused on match suppression (Miller and Desimone, 1993, 1994), and sometimes only match suppression is reported without any match enhancement (Fahy et al., 1993). This match suppression could arise from a number of different physiological mechanisms. Here we demonstrate how network interactions could result in match suppression as an indirect effect of I_{NCM}. In these network simulations, lateral inhibition from neurons undergoing match enhancement causes match suppression in other neurons. Figure 8 demonstrates match suppression in a subset of neurons within the network simulation. In this example, input from stim A activates both pyramidal cells, similar to the example in Figure 7. These pyramidal cells main-

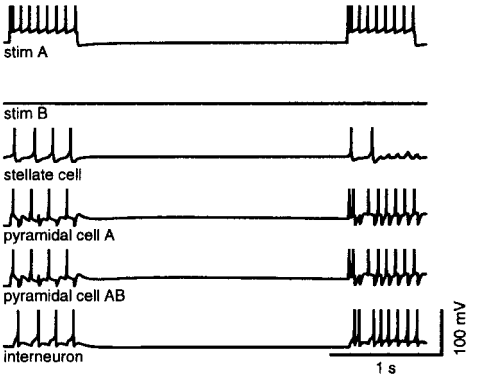

Figure 8. Network simulation demonstrating match suppression attributable to network interactions. The network contains the same set of neurons described in Figure 7. Input from *stim A* activates both pyramidal cell A and pyramidal cell AB for 600 msec and causes subthreshold depolarization during the delay period. This results in increased depolarization and in a greater number of spikes in both pyramidal cells when input from stim A arrives during the match period. However, in contrast to Figure 7, stronger inhibitory connectivity to the stellate cell causes this neuron to show match suppression (i.e., it generates fewer spikes in response to the match stimulus than to the preceding sample stimulus). Action potentials are truncated in this figure. Synaptic conductances are summarized in Table 9.

tain subthreshold depolarization during the delay period, which causes match enhancement. However, the stellate neuron in this example has stronger inhibitory connections from the inhibitory interneuron. This results in match suppression in the stellate cell because of the feedback inhibition activated by the pyramidal cells showing match enhancement. The synaptic conductances are summarized in Table 9.

Non-match enhancement and suppression

Studies on spiking activity in the entorhinal cortex in rats used a continuous delayed non-match to sample paradigm in which each stimulus is simultaneously a sample stimulus for the next trial and a match stimulus for the preceding trial (Young et al., 1997). A continuous recognition task has also been used in monkeys (Fahy et al., 1993), in which stimuli were both sample and match stimuli (although that task required a response to a familiar stimulus even if there were many intervening stimuli since its previous presentation). In those continuous matching tasks, only match enhancement and match suppression could be quantified. However, other studies in monkeys have used discrete trial matching tasks in which each trial involves presentation of a single sample stimulus followed by a delay period during which several test stimuli can be presented sequentially for matching (Miller and Desimone, 1994; Suzuki et al., 1997). After the matching stimulus appears, there is an intertrial interval before the next sample stimulus is presented (Miller and Desimone, 1994; Suzuki et al., 1997). In these studies, the response during the sample period can be used as a baseline and it is possible to differentiate match suppression from non-match enhancement. In non-match enhancement, presentation of stimuli during the match stimulus induces more spikes on average when the stimulus does not match the stimulus presented during the sample period. In non-match suppression, presentation of a stimulus during the test period generates fewer spikes if it does not match the stimulus during the sample period.

Figure 9 shows examples of non-match enhancement and non-match suppression. Here the features of the nonselective cell

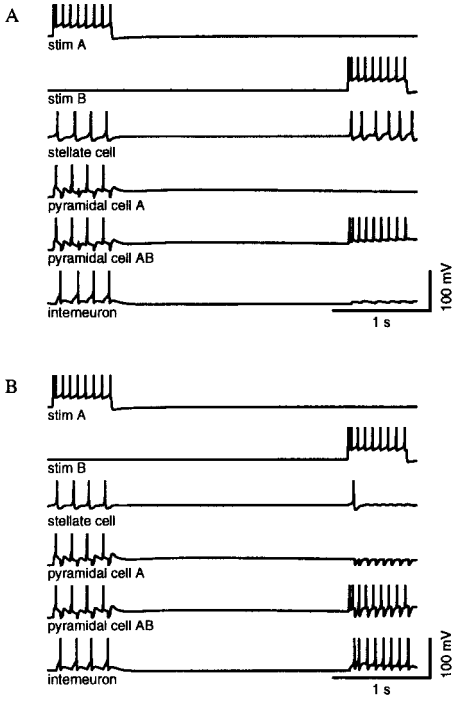

Figure 9. Network simulation demonstrating non-match enhancement and non-match suppression. The network contains the same set of neurons described in previous figures. *A*, Non-match enhancement (same network as Fig. 8). During the sample period, input from *stim A* activates both pyramidal cell A and pyramidal cell AB for 600 msec and causes sustained subthreshold depolarization during the delay period. During the match period, input from stim B activates only pyramidal cell AB. This results in a greater number of spikes in pyramidal cell AB. The interneuron has strongest input from the silent stim A, which results in less feedback inhibition during the test stimulus. Increased input from pyramidal cell AB and decreased inhibition from the interneuron causes a greater response in the stellate cell for the non-match condition. Action potentials are truncated in both parts of this figure. Synaptic conductances are the same as in Table 9. *B*, Non-match suppression (same network as Fig. 9). This example has the same features as Figure 8*A*, except that there is a stronger excitatory connection from pyramidal cell AB to the inhibitory interneuron. The result is that the greater activity of pyramidal cell AB during the test presentation causes greater feedback inhibition and a net decrease in the spiking activity of the stellate cell during the non-match period. Synaptic conductances are summarized in Table 10.

(pyramidal cell AB) play an important role along with the I_{NCM} current in inducing these effects. In Figure 9*A*, non-match enhancement occurs in the stellate cell from a change in the relative level of excitation and inhibition in the network. Synaptic parameters are the same as in Figure 8 (Table 9). During the sample period, input neuron stim A activates both pyramidal cell A and pyramidal cell AB; this causes strong activation of the inhibitory interneuron, resulting in a small number of spikes in the stellate cell. During the match period, activation of input neuron stim B only activates the nonselective pyramidal cell AB. This neuron shows a match enhancement attributable to subthreshold depolarization during the delay period, giving stronger excitatory input to the stellate cell, but the lack of spiking in pyramidal cell A results in less spiking of the interneuron, giving less inhibitory input to the stellate cell. The combination of these effects results in a stronger response in the stellate cell for the non-match input (non-match enhancement). In a separate simulation, when given input from stim B followed by repetition of stim B input, the

network responds both times with five spikes, as opposed to six spikes for the stim B response after stim A. Thus, the network shows non-match enhancement both in a comparison of the second (test) stimulus with the first (sample) stimulus and when comparing the test response in match versus non-match conditions. As shown in Figure 9*B*, altering the simulation by adding an excitatory connection from pyramidal cell AB (instead of pyramidal cell A) to the interneuron can cause non-match suppression instead of non-match enhancement. Here the match enhancement in pyramidal cell AB causes greater interneuron spiking, which results in an overall decrease in spiking activity in the stellate cell during the non-match trial. The synaptic weights for this simulation are summarized in Table 10.

Sensitivity to changes in synaptic conductances

The sensitivity of the networks to changes in synaptic parameters was analyzed extensively in simulations changing the magnitude of synaptic conductances (listed in Tables 8–10). In 48 simulations, each of the categories of synaptic conductances listed in Tables 8–10 for connections between stellate cells, pyramidal cells, and inhibitory interneurons was changed one at a time. Thus, each of the six values in the table was tested, as well as the related NMDA value for excitatory cells and the related $GABA_B$ value for inhibitory connections. For each value, the network was tested with a 20% increase and a 20% decrease in that value. The category of neuronal response of the stellate cell was then evaluated to see if it correctly produced a match enhancement, match suppression, non-match enhancement, or non-match suppression. An increase of 20% of any synaptic connection strength produced the correct response in every one of 24 tests. For a decrease of 20%, all except 1 of the 24 tests gave a correct type of output. In that single case, only a 5% decrease could be tolerated. Thus, 47 out of 48 tests gave a correct type of output for a 20% change in synaptic conductance. In separate simulations, the sensitivity to "background" cellular spiking was addressed (Alonso and Garcia-Austt, 1987; Stewart et al., 1992). In *in vivo* recordings by Mizumori et al. (1992), it was found that 60% of the cells fired at a rate of 0–1 Hz. With a cellular background rate of 0.5 Hz in the simulation, delay activity as well as match- and non-match enhancement and suppression were produced just as reported above without the background.

Repetition suppression

In addition to the role of I_{NCM} in working memory phenomena, there are a number of additional mechanisms that can play a role. We have not explored the full range of synaptic mechanisms for these phenomena but have explored the potential role of the calcium-activated potassium current I_{KAHP} in suppression of the response during stimulus repetition. Suppression of response has been shown in unit recordings from inferotemporal neurons during repetitive presentation of visual stimuli (Miller et al., 1991). This repetition suppression and the match suppression described above could arise from activation of the I_{KAHP} current. This has been analyzed previously in more abstract simulations of the inferotemporal cortex (Sohal and Hasselmo, 2000). However, the long interval between the sample presentation and the match presentation in most experiments (Suzuki et al., 1997; Young et al., 1997) requires a rather slow time constant for the I_{KAHP} in the model. Most of the simulations presented here have included an I_{KAHP} with a more standard time constant of decay of 100 msec. However, a number of studies have shown that a component of the I_{KAHP} can have a time constant significantly slower than 100 msec (Alonso and Klink, 1993; Storm, 1993; Saar et al., 2001). If we include a current with a slower time constant, we can account for some match suppression and repetition suppression. In these simulations (data not shown), repeated activation of a single cell causes less spiking on subsequent presentations because of the residual potassium current persisting after the first activation of the cell. This results from the calcium influx during initial spiking, which activates potassium currents with a slow time course.

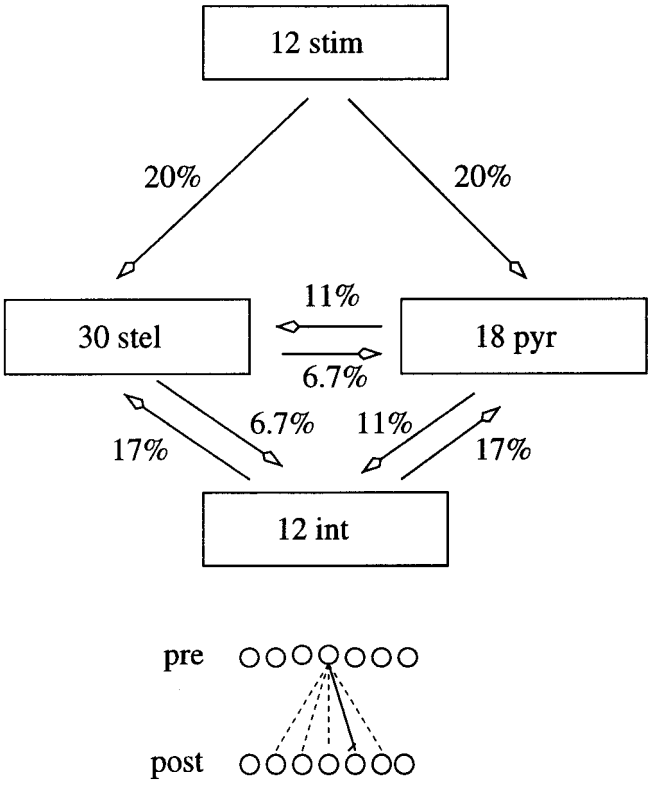

Figure 10. Connectivity in the larger network simulation. *Top*, This figure shows a schematic representation of the population of 12 input cells, 30 stellate cells, 18 pyramidal cells, and 18 inhibitory interneurons. The percentage of synaptic connectivity between the different populations is summarized next to the appropriate *arrow*. The individual location of and number of connections for each cell were determined randomly. The strength and number of connections in the network are summarized in Tables 11 and 12. *Bottom*, Illustration of the constraints on connectivity between regions. Presynaptic neurons could contact postsynaptic neurons of the same index and within a window of varying width (width 2 shown here). *Dotted lines* represent potential connections allowed by the window. The *solid line* represents the connection that was randomly selected.

Multiple different matching phenomena arise from connectivity in a large network

The preceding section showed simple examples of small-scale network interactions that could underlie phenomena observed in unit recordings from the entorhinal cortex during DNMS and DMS tasks, including match suppression and non-match enhancement and suppression. This section demonstrates that these types of phenomena can arise in a simple, natural manner because of connectivity chosen randomly within constraints on number, distribution, and weight in a larger-scale simulation of interacting populations of neurons in the entorhinal cortex. The connectivity properties of this larger network are summarized in Materials and Methods, in Figure 10, and in Tables 11 and 12. This larger

Table 12. Larger network

Pre-cell	Stim	Stel	Pyr	Int
Post-cell				
Stel	73	0	60	60
Pyr	43	36	0	36
Int	0	24	24	0

The number of connections between different cell populations is shown.

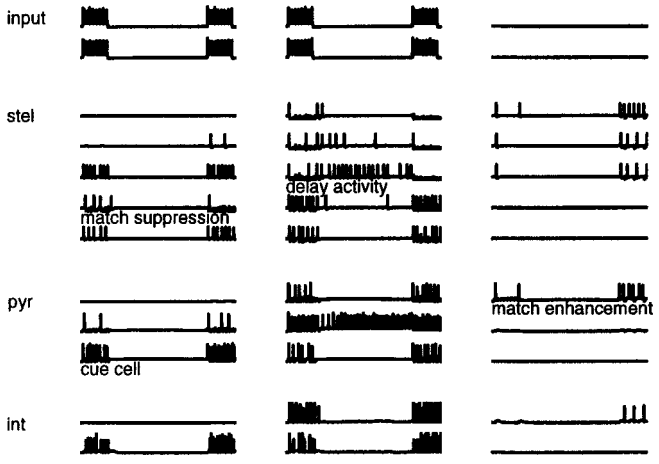

Figure 11. Overview of activity in the larger, random connected network during a matching trial (repeated activation of input neurons 4–7). Neurons on the left side of the arrays received input from input neurons 4–7, but this input could also influence activity in neurons receiving primary input from neurons 8–11. Connectivity within the network was assigned randomly with the general constraint that it would primarily contact nearby cells and have the connection strengths listed in Table 11. This results in a diverse range of firing patterns during this match trial, without selective tuning of specific connections. The random number and type of interconnections results in a range of experimentally observed phenomena, including match enhancement (pyr 12), match suppression (stel 13), pure delay activity (stel 17), and pure cue activity (pyr 8). Obtaining these phenomena did not require selective tuning of specific synaptic connections.

network simulation was tested for responses to matching stimuli (in which the first presentation of stimulus pattern A is followed by another presentation of the same stimulus pattern) and to non-matching stimuli (in which presentation of stimulus pattern A is followed by presentation of a different stimulus pattern B). This simulation uses the relative percentage of cell types found in experimental studies (Alonso and Klink, 1993).

Activity during matching

Connectivity chosen randomly within constraints on number, distribution, and weight in the larger network simulation resulted in a range of response properties resembling neuronal recordings during presentation of matching stimuli (repeated activation of input neurons 4–7), as shown in Figure 11. Figure 11 shows the membrane potentials of some individual simulated neurons in the network, which included 12 input neurons, 30 stellate cells, 18 pyramidal cells, and 12 interneurons. Synaptic connectivity was assigned randomly within general constraints mapping input to particular numerical ranges of neurons in the network. Neurons in the *center* and *left columns* of Figure 11 received input from input neurons 4–7, but the input from neurons 4–7 also contacted other neurons receiving primary input from neurons 8–11. The number of connections within the network was assigned randomly between the pyramidal cells, stellate cells, and interneurons, with the constraint of being local. As shown in Figure 11, the connectivity chosen randomly within constraints on number, distribution, and weight results in a diverse range of firing patterns during this match trial, including phenomena corresponding to most of the cell types observed during unit recording in awake behaving animals (Suzuki et al., 1997; Young et al., 1997), including match enhancement (pyr 12), match suppression (stel 13), pure delay activity (stel 17), and pure cue activity (pyr 8). Note that in unit recording experiments done in the entorhinal cortex of awake animals, it has not been possible to distinguish stellate cells from pyramidal cells. Thus, unit properties described in chronic recordings from awake animals could reflect recordings of either of the different morphological subtypes modeled in these simulations. There was no uncontrolled spreading of activity between the neurons primarily representing input A and those primarily representing input B. However, the inputs from neurons 4–7 (input A) and 8–11 (input B) had overlapping inputs to some of the cells in the network. Therefore, the match enhancement shown here can be analyzed to determine whether it is selective for one input (e.g., input A) without appearing for the overlapping input (e.g., input B). There were neurons that showed selective enhancement, and this selective enhancement has been quantified in a larger range of networks discussed below.

This simulation demonstrates that these neuronal response subtypes can be obtained because of connectivity chosen randomly within constraints for defined network interactions between individual subclasses of neurons. They can result from an interaction of specific intrinsic cellular properties (including the I_{NCM} and I_{KAHP}) with the excitatory and inhibitory interactions of neurons within different populations. The specific example networks shown in the preceding section arise in a simple and natural manner from interactions of neurons within a larger network, without complicated fine tuning of individual synaptic connections.

Activity during non-matching

Similar to the result for the matching phenomena, the phenomena observed during non-match trials can also be obtained in a simple manner in the larger network simulation with connections chosen randomly within constraints on the number, distribution, and weight of synapses. The response of the larger network to a non-match is shown in Figure 12. Here, the network initially receives activation of input neurons 4–7. Then, after a delay period, the network receives activation of input neurons 8–11. The neurons in the *columns* on the *left* of Figure 12 primarily receive connections from neurons 4–7, but there is some activation of neurons receiving primary input from neurons 8–11. Similarly, the input from neurons 8–11 primarily activates a different set of neurons but causes some activation of neurons getting input from 4–7. The neurons receiving greater input from both sets of input neurons correspond to the nonselective cells used in the example simulations above (pyramidal cell AB) and play an important role in mediating some of the non-match phenomena that can be observed in the network. As shown in Figure 12, this network shows examples of the experimental phenomena observed in unit recordings from awake animals during non-matching, including non-match enhancement (stel 20), non-match suppression (stel 18), delay activity (stel 17), input specificity (pyr 13), and input non-specificity (pyr 11). Thus, the specific examples of circuitry underlying non-match phenomena shown in the previous section arise in a simple manner within a

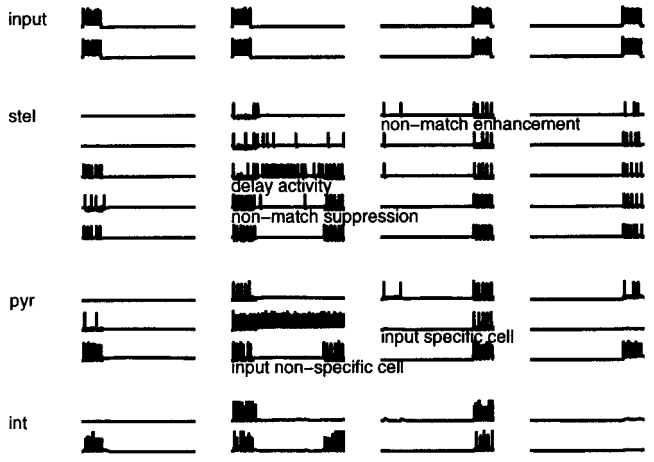

Figure 12. Activity in the larger, random connected network during a non-match trial (activation of input neurons 4–7 was followed after a delay by activation of input neurons 8–11). Membrane potentials are shown for the component neurons in the network during the non-matching stimulation. Neurons on the left side of the arrays primarily received connections from input neurons 4–7, and a separate set of neurons primarily received connections from input neurons 8–11, but the random overlap of input and connectivity between these two populations of neurons allows interactions resulting in non-match phenomena. The connectivity selected randomly within constraints of number, distribution, and weight resulted in a range of experimentally observed phenomena, including non-match enhancement (stel 20), non-match suppression (stel 18), delay activity (stel 17), input specificity (pyr 13), and input nonspecificity (pyr 11).

larger network because of random selection of internal connectivity within constraints rather than because of selective tuning of individual synaptic connections.

Sensitivity of large simulation to connectivity changes

In separate simulations, we also tested variations in the number and distribution of synaptic connections between different populations of neurons. We varied both number of connections (increasing by 50, 100, and 150%) and window width (unchanged, one cell wider on both sides, or two cells wider on both sides). For each match or non-match simulation, we counted how many of the classes of neuronal response were still present in the simulation. The classes considered were enhancement, suppression, delay activity, cue (match), or stimulus specificity (non-match) (i.e., four classes). The average number of classes appearing in 18 tests was 3.3 (out of 4 classes). In additional simulations, the sensitivity to background cellular spiking was tested using the same background rate of 0.5 Hz described above. In these conditions of background activity, all categories of neural response types still appeared in both the match and non-match conditions.

To analyze the specificity of the enhancement for the sample stimulus, we quantified whether cells showing enhancement to one of the overlapping stimuli (stimulus A or stimulus B) would show selective enhancement for only the match stimulus. That is, if the cell responds to stimulus A and shows match enhancement to the second presentation of stimulus A, to be selective it must not show enhancement to the non-matching stimulus B that overlaps with stimulus A. This analysis was only performed for cells that responded to both stimulus A and stimulus B as sample stimuli. We tested the selectivity of match enhancement for 10 different networks. There was an average of 8.3 cells per network showing match enhancement, out of which an average of 1.7 cells showed selective match enhancement as defined above. Thus, ~20% of cells showing match enhancement were selective for just one sample stimulus. The remaining 80% either did not respond to the other overlapping stimulus or showed nonselective enhancement. For the selective enhancement cells, the sample stimulus evoked an average of 6.6 spikes and the matching stimulus evoked an average of 9.7 spikes. For these same selective enhancement cells, the overlapping sample stimulus evoked an average of 7.4 sample spikes but the overlapping non-matching stimulus evoked an average of 4.4 spikes.

DISCUSSION

The simulations presented here demonstrate that the muscarinic activation of the calcium-sensitive nonspecific cation current I_{NCM} could underlie the plateau potentials and bursting activity observed with intracellular recording from pyramidal cells in slice preparations of the entorhinal cortex (Klink and Alonso, 1997a,b; Magistretti et al., 2001) (Magistretti, Ma, Shalinsky, and Alonso, unpublished observations). Network simulations support the theory that the cholinergic activation of this current could underlie properties of the unit activation observed in the entorhinal cortex during performance of continuous delayed non-match to sample tasks in rats (Young et al., 1997) and during performance of delayed match to sample tasks by monkeys (Miller et al., 1993; Suzuki et al., 1997). In particular, as shown in Figures 3, 7, 11, and 12, the current directly induces sustained spiking during the delay period of the task, as well as the enhancement of spiking during the matching period relative to the response to the same stimulus during the sample period. As shown in Figure 4, this sustained spiking activity can withstand short periods of hyperpolarization which could result from distractor stimuli. The muscarinic enhancement of the I_{NCM} current may be further enhanced by the blockade of potassium currents, which makes the cell more electrotonically compact (Menschik and Finkel, 1998) (Alonso, unpublished observations). This would allow somatic generated spikes to more strongly activate dendritic calcium channels, and thereby further enhance the activation of dendritic I_{NCM} currents.

Network interactions between cells could underlie additional phenomena observed in unit recording from awake animals (Suzuki et al., 1997; Young et al., 1997). These phenomena include: (1) match suppression (Figs. 8, 11), which could result from inhibition by interneurons driven by other neurons undergoing match enhancement; (2) non-match enhancement (Figs. 9*A*, 12) which could result from strong excitatory input from nonselective cells; and (3) non-match suppression (Figs. 9*B*, 12), which could result from greater activation of inhibitory interneurons by nonselective cells. These are examples of potential network mechanisms for the firing properties of neurons *in vivo*, but do not exclusively cover all the possible mechanisms. In the larger network simulation, these response properties arose naturally from the randomly connected network, without any procedure focused on tuning of synaptic connections, suggesting that a network with the intrinsic phenomena described here easily manifests the various response properties described in unit recording from behaving animals. When classifying cells according to their firing properties, cells can be classified as stimulus selective or nonselective. Our simulations may provide one explanation for the role of the nonselective cells. In the non-match simulations, the differential action of the selective and the nonselective cells and their connectivity to interneurons provide a mechanism for causing non-match enhancement and suppression activity.

Other potential mechanisms for match suppression

In the simulations presented here, match suppression arises because of inhibition from neurons showing match enhancement attributable to I_{NCM} or attributable to activation of slow I_{KAHP}. However, other potential mechanisms could underlie the phenomena of match suppression. It is possible that during the initial viewing of a stimulus, cholinergic modulation is at high levels, whereas subsequent viewing of a matching stimulus might cause feedback suppression of cholinergic modulation, which decreases the neuronal activity in response to the stimulus (Sohal and Hasselmo, 2000). This type of match suppression should be sensitive to cholinergic blockade. In contrast, match suppression might also arise from the self-organization of feedforward connections with a combination of synaptic enhancement and synaptic depression (Sohal and Hasselmo, 2000; Bogacz et al., 2001). These mechanisms might be less sensitive to cholinergic blockade, and this possibility is supported by the absence of a change in match suppression with local infusion of cholinergic antagonists during recording in the inferotemporal cortex (Miller and Desimone, 1993). In these cases, match suppression may be more sensitive to increases in cholinergic influences because of local infusion of the acetylcholinesterase blocker physostigmine. Some studies describe an active reset mechanism such that consecutive presentation of a stimulus as a sample does not induce match suppression, even if the intervening match presentations show suppression (Miller et al., 1991, 1993). This phenomena could arise if spike frequency accommodation mediates match suppression and higher levels of acetylcholine during the sample phase suppress this accommodation. In this case, scopolamine should block the active reset mechanism. The muscarinic antagonist scopolamine should block match enhancement mediated by I_{NCM}, but the lack of an effect of scopolamine on match suppression does not necessarily rule out involvement of I_{NCM} in match suppression during control conditions. Cholinergic blockade by scopolamine might decrease I_{NCM}, but would simultaneously unmask several potassium currents normally blocked by muscarinic cholinergic receptor activation, which could thereby increase AHPs and increase the resulting match suppression in experimental studies. In addition, cholinergic blockade could also enhance the magnitude of calcium currents reduced by cholinergic modulation (Magistretti et al., 2001).

Cholinergic modulation of entorhinal cortical function

As yet no data have specifically tested the involvement of I_{NCM} in delay activity *in vivo*, but research does support cholinergic modulation of such activity. If cholinergic activation of I_{NCM} is important to provide intrinsic mechanisms for self-sustained spiking activity, then blockade of this muscarinic cholinergic activation should reduce sustained spiking activity during the delay period and match enhancement. This effect of muscarinic antagonists could underlie the behavioral impairments in delayed matching tasks seen with systemic injections of muscarinic antagonists (Bartus and Johnson, 1976; Penetar and McDonough, 1983). In addition to this role in short-term memory function, sustained activity in the entorhinal cortex could also be very important for effective encoding of long-term representations through synaptic modification in the hippocampal formation. If it plays this role in buffering information for encoding into long-term memory, then blockade of sustained entorhinal activity by muscarinic antagonists could also underlie the impairments of encoding for subsequent recognition or recall observed with local infusion of the antagonist scopolamine into the perirhinal cortex in monkeys (Tang et al., 1997) or with systemic injections of scopolamine in monkeys (Aigner and Mishkin, 1986; Aigner et al., 1991) and human subjects (Ghonheim and Mewaldt, 1975; Peterson, 1977).

Relation to cholinergic modulation in the prefrontal cortex

Intracellular recording has demonstrated that cholinergic modulation also induces sustained depolarizations after spiking in slice preparations of the prefrontal cortex (Andrade, 1991; Haj-Dahmane and Andrade, 1996, 1998). The current in the prefrontal cortex also has calcium-sensitive properties but differs from the current described here in that it is voltage dependent. These data were used to support previous models of working memory function that are dependent on afterdepolarization (Lisman and Idiart, 1995; Jensen and Lisman, 1996, 1998). These previous models focused on the simultaneous working memory for multiple stimuli and did not incorporate the same level of biophysical detail as the models presented here, but they used essentially the same mechanism described here. Muscarinic cholinergic modulation of currents in prefrontal cortical neurons could therefore also contribute to sustained spiking activity, which has been observed during many different types of delayed match to sample tasks during recording from the prefrontal cortex (Fuster, 1973; Wilson et al., 1993; Miller et al., 1996).

Possible relationship to other models of working memory

A number of other models have been developed for sustained activity during working memory function. Most of these models focus on the role of synaptic connectivity in maintaining network activity. One set of studies has focused on the role of synaptic NMDA receptors in allowing previously activated neurons to remain active because of the fact that NMDA receptors will cause stronger currents in neurons that are already depolarized (Lisman et al., 1998; Durstewitz et al., 2000). The slower time course of NMDA receptor currents has also been emphasized in these models, because these slower dynamics could allow networks to maintain sustained spiking activity with lower firing rates (Fransén and Lansner, 1995; Seung, 1996; Lisman et al., 1998). The neuromodulatory effects of dopamine on sustained activity were examined in great detail with a simulation containing biophysically detailed representations of prefrontal cortical neurons (Durstewitz et al., 2000). That simulation focused on the dopaminergic enhancement of persistent sodium currents (NaP) and NMDA currents, showing that those effects enhanced the stability of sustained network activity, although they could not allow single neurons to sustain activity. Sustained activity dependent on the pattern of synaptic connectivity may be more appropriate for encoding of familiar stimuli, whereas intrinsic cellular mechanisms could mediate sustained activity for novel stimuli. Consistent with this, functional magnetic resonance imaging suggests that the prefrontal cortex shows greater activation during working memory for familiar stimuli, whereas medial temporal cortices show stronger activity during working memory for novel stimuli (Stern et al., 2001). The intrinsic mechanisms described in here are not incompatible with the existence of synaptic mechanisms for sustained activity, although they may result in differences in spike timing and stability properties. Explicit representation of the cellular mechanisms that could contribute to spiking activity patterns during delayed match to sample tasks will allow more detailed experimental analysis and comparison of the candidate mechanisms for these activity patterns.

REFERENCES

Aigner TG, Mishkin M (1986) The effects of physostigmine and scopolamine on recognition memory in monkeys. Behav Neural Biol 45:81–87.

Aigner TG, Walker DL, Mishkin M (1991) Comparison of the effects of scopolamine administered before and after acquisition in a test of visual recognition memory in monkeys. Behav Neural Biol 55:61–67.

Alonso A, Garcia-Austt E (1987) Neuronal sources of theta rhythm in the entorhinal cortex of the rat. II. Phase relations between unit discharges and theta field potentials. Exp Brain Res 67:502–509.

Alonso A, Klink R (1993) Differential electroresponsiveness of stellate and pyramidal-like cells of medial entorhinal cortex layer II. J Neurophysiol 70:128–143.

Alonso A, de Curtis M, Llinas R (1990) Postsynaptic Hebbian and non-Hebbian long-term potentiation of synaptic efficacy in the entorhinal cortex in slices and in the isolated adult guinea pig brain. Proc Natl Acad Sci USA 87:9280–9284.

Andrade R (1991) Cell excitation enhances muscarinic cholinergic responses in rat association cortex. Brain Res 548:81–93.

Bartus RT, Johnson HR (1976) Short-term memory in the rhesus monkey: disruption from the anti-cholinergic scopolamine. Pharmacol Biochem Behav 5:39–46.

Bhalla U, Bower J (1993) Exploring parameter space in detailed single neuron models: simulations of the mitral and granule cells of the olfactory bulb. J Neurophysiol 69:1948–1965.

Bogacz R, Brown MW, Giraud-Carrier C (2001) Model of familiarity discrimination in the perirhinal cortex. J Comput Neurosci 10:5–23.

Bower JM, Beeman D (1995) The book of GENESIS: exploring realistic neural models with the GEneral NEural SImulation System. New York: Springer-Verlag.

Bruehl C, Wadman WJ (1999) Calcium currents in acutely isolated stellate and pyramidal neurons of rat entorhinal cortex. Brain Res 816:554–562.

DeSchutter E, Bower JM (1994) An active membrane model of the cerebellar Purkinje cell. I. Simulation of current clamps in slice. J Neurophysiol 71:375–400.

Dickson CT, Magistretti J, Shalinsky MH, Fransn E, Hasselmo M, Alonso A (2000) Properties and role of I_h in the pacing of subthreshold oscillations in entorhinal cortex layer II neurons. J Neurophysiol 83:2562–2579.

Durstewitz D, Seamans JK, Sejnowski TJ (2000) Dopamine-mediated stabilization of delay-period activity in a network model of prefrontal cortex. J Neurophysiol 83:1733–1750.

Fahy FL, Riches IP, Brown MW (1993) Neuronal activity related to visual recognition memory: long term memory and the encoding of recency and familiarity information in the primate anterior and medial inferior temporal and rhinal cortex. Exp Brain Res 96:457–472.

Fransén E, Lansner A (1995) Low spiking rates in a population of mutually exciting pyramidal cells. Network 6:271–288.

Fransén E, Dickson CT, Magistretti J, Alonso AA, Hasselmo ME (1998) Modeling the generation of subthreshold membrane potential oscillations of entorhinal cortex layer II stellate cells. Soc Neurosci Abstr 24:814.5.

Fransén E, Wallenstein GV, Alonso A, Dickson CT, Hasselmo ME (1999a) A biophysical simulation of intrinsic and network properties of entorhinal cortex. Neurocomputing 26–27:375–380.

Fransén E, Alonso A, Hasselmo ME (1999b) Intrinsic properties of rat entorhinal cells relevant to working memory. Soc Neurosci Abstr 25:725.6.

Fransén E, Alonso AA, Hasselmo ME (2000) Cellular and synaptic mechanisms of match enhancement and depression in DMS working memory tasks involving entorhinal cortex. Soc Neurosci Abstr 26:596.6.

Fuster JM (1973) Unit activity in prefrontal cortex during delayed-response performance: neuronal correlates of transient memory. J Neurophysiol 36:61–78.

Ghonheim MM, Mewaldt SP (1975) Effects of diazepam and scopolamine on storage, retrieval and organization processes in memory. Psychopharmacologia 44:257–262.

Gloveli T, Egorov AV, Schmitz D, Heinemann U, Muller W (1999) Carbachol-induced changes in excitability and $[Ca^{2+}]_i$ signaling in projection cells of medial entorhinal cortex layers II and III. Eur J Neurosci 11:3626–3636.

Haj-Dahmane S, Andrade R (1996) Muscarinic activation of a voltage-dependent cation nonselective current in rat association cortex. J Neurosci 16:3848–3861.

Haj-Dahmane S, Andrade R (1998) Ionic mechanism of the slow after-depolarization induced by muscarinic receptor activation in rat prefrontal cortex. J Neurophysiol 80:1197–1210.

Hines M (1984) Efficient computation of branched nerve equations. Int J Biomed Comput 15:69–79.

Jensen O, Lisman JE (1996) Novel lists of 7 ± 2 known items can be reliably stored in an oscillatory short-term memory network: interaction with long-term memory. Learn Mem 3:257–263.

Jensen O, Lisman JE (1998) An oscillatory short-term memory buffer model can account for data on the Sternberg task. J Neurosci 18:10688–10699.

Jones RS, Buhl EH (1993) Basket-like interneurons in layer II of the entorhinal cortex exhibit a powerful NMDA-mediated synaptic excitation. Neurosci Lett 149:35–39.

Klink R, Alonso A (1993) Ionic mechanisms for the subthreshold oscillations and differential electroresponsiveness of medial entorhinal cortex layer II neurons. J Neurophysiol 70:144–157.

Klink R, Alonso A (1997a) Muscarinic modulation of the oscillatory and repetitive firing properties of entorhinal cortex layer II neurons. J Neurophysiol 77:1813–1828.

Klink R, Alonso A (1997b) Ionic mechanisms of muscarinic depolarization in entorhinal cortex layer II neurons. J Neurophysiol 77:1829–1843.

Klink R, Alonso A (1997c) Morphological characteristics of layer II projection neurons in the rat medial entorhinal cortex. Hippocampus 7:571–583.

Leonard BW, Amaral DG, Squire LR, Zola-Morgan S (1995) Transient memory impairment in monkeys with bilateral lesions of the entorhinal cortex. J Neurosci 15:5637–5659.

Lisman JE, Idiart MA (1995) Storage of 7 ± 2 short-term memories in oscillatory subcycles. Science 267:1512–1515.

Lisman JE, Fellous JM, Wang XJ (1998) A role for NMDA-receptor channels in working memory. Nat Neurosci 1:273–275.

Magistretti J, Ragsdale D, Alonso A (1999) High conductance sustained single-channel activity responsible for the low-threshold persistent Na^+ current in entorhinal cortex neurons. J Neurosci 19:7334–7341.

Magistretti J, Ma L, Schalinsky MH, Alonso A (2001) Activity-dependent homeostatic regulation of a muscarinic activated non-specific cation current in entorhinal cortex layer-II neurons. Soc Neurosci Abstr, in press.

McCormick DA, Huguenard JR (1992) A model of the electrophysiological properties of thalamocortical relay neurons. J Neurophysiol 68:1384–1400.

Menschik ED, Finkel LH (1998) Neuromodulatory control of hippocampal function: towards a model of Alzheimer's disease. Artif Intell Med 13:99–121.

Miller EK, Desimone R (1993) Scopolamine affects short-term memory but not inferior temporal neurons. NeuroReport 4:81–84.

Miller EK, Desimone R (1994) Parallel neuronal mechanisms for short-term memory. Science 263:520–522.

Miller EK, Lin L, Desimone R (1991) A neural mechanism for working and recognition memory in inferior temporal cortex. Science 254:1377–1379.

Miller EK, Lin L, Desimone R (1993) Activity of neurons in anterior inferior temporal cortex during a short-term memory task. J Neurosci 13:1460–1478.

Miller EK, Erickson CA, Desimone R (1996) Neural mechanisms of visual working memory in prefrontal cortex of the macaque. J Neurosci 16:5154–5167.

Mizumori SJ, Ward KE, Lavoie AM (1992) Medial septal modulation of entorhinal single unit activity in anesthetized and freely moving rats. Brain Res 570:188–197.

Otto T, Eichenbaum H (1992) Complementary roles of orbital prefrontal cortex and the perirhinal-entorhinal cortices in an odor-guided delayed non-matching to sample task. Behav Neurosci 106:763–776.

Penetar DM, McDonough Jr JH (1983) Effects of cholinergic drugs on delayed match-to-sample performance of rhesus monkeys. Pharmacol Biochem Behav 19:963–967.

Peterson RC (1977) Scopolamine induced learning failures in man. Psychopharmacology 52:283–289.

Saar D, Grossman Y, Barkai E (2001) Long-lasting cholinergic modulation underlies rule learning in rats. J Neurosci 15:1385–1392.

Seung HS (1996) How the brain keeps the eyes still. Proc Natl Acad Sci USA 93:13339–13344.

Sohal VS, Hasselmo ME (2000) A model for experience-dependent changes in the responses of inferotemporal neurons. Network 11:169–190.

Stern CE, Sherman SJ, Kirchhoff BA, Hasselmo ME (2001) Medial temporal and prefrontal contributions to working memory tasks with novel and familiar stimuli. Hippocampus 11:337–346.

Stewart M, Quirk GJ, Barry M, Fox SE (1992) Firing relations of medial entorhinal neurons to the hippocampal theta rhythm in urethan anesthetized and walking rats. Exp Brain Res 90:21–28.

Storm JF (1993) Functional diversity of K^+ currents in hippocampal pyramidal neurons. Semin Neurosci 5:79–92.

Suzuki WA, Miller EK, Desimone R (1997) Object and place memory in the macaque entorhinal cortex. J Neurophysiol 78:1062–1081.

Tang Y, Aigner TG (1996) Release of cerebral acetylcholine increases

during visually mediated behavior in monkeys. NeuroReport 7:2231–2235.
Tang Y, Mishkin M, Aigner TG (1997) Effects of muscarinic blockade in perirhinal cortex during visual recognition. Proc Natl Acad Sci USA 94:12667–12669.
Traub RD, Wong RKS, Miles R, Michelson H (1991) A model of a CA3 pyramidal neuron incorporating voltage-clamp data on intrinsic conductances. J Neurophysiol 66:635–650.
Traub RD, Jefferys JG, Miles R, Whittington MA, Toth K (1994) A branching dendritic model of a rodent CA3 pyramidal neurone. J Physiol (Lond) 481:79–95.
White JA, Klink R, Alonso A, Kay AR (1998) Noise from voltage-gated ion channels may influence neuronal dynamics in the entorhinal cortex. J Neurophysiol 80:262–269.
Wilson FA, Scalaidhe SP, Goldman-Rakic PS (1993) Dissociation of object and spatial processing domains in primate prefrontal cortex. Science 260:1955–1958.
Young BJ, Otto T, Fox GD, Eichenbaum H (1997) Memory representation within the parahippocampal region. J Neurosci 17:5183–5195.
Zador A, Koch C, Brown TH (1990) Biophysical model of a Hebbian synapse. Proc Natl Acad Sci USA 10:6718–6772.
Zola-Morgan S, Squire LR, Clower RP, Rempel NL (1993) Damage to the perirhinal cortex exacerbates memory impairment following lesions to the hippocampal formation. J Neurosci 13:251–265.